The specific molecular signature of dissolved organic matter extracted from different arctic plant species persists after biodegradation

Alienor Allain [a,*], Marie A. Alexis [a], Maxime C. Bridoux [b], Liudmila S. Shirokova [c,d], Dahédrey Payandi-Rolland [c], Oleg S. Pokrovsky [c,e], Maryse Rouelle [a]

[a] Sorbonne Universite, CNRS, EPHE, UMR METIS, 75252, Paris, France
[b] CEA/DAM/DIF, Bruyères-le-Châtel, 91297, Arpajon, France
[c] Geoscience and Environment Toulouse, UMR 5563 CNRS, University of Toulouse, 14 Avenue Edouard Belin, 31400, Toulouse, France
[d] N. Laverov Federal Center for Integrated Arctic Research, UrB RAS, 23 Nab Severnoi Dviny, 163000 Arkhangelsk, Russia
[e] BIO-GEO-CLIM Laboratory, Tomsk State University, 634050, Tomsk, Russia

A B S T R A C T

Dissolved organic matter (DOM) is a small but very reactive pool of organic matter (OM) in the environment. Its role is related to its composition, which depends on its source. In soils, vegetation is the main source of DOM, and biodegradation is the main regulating mechanism. This study aims to characterise DOM produced by contrasted arctic vegetation species and their biodegradation products.

The water-extractable organic matter (WEOM) was produced from *C. stellaris* (lichen), *E. vaginatum* (sedge), *A. polifolia* (dwarf evergreen shrub) and *B. nana* (deciduous dwarf shrub). The WEOM were inoculated with a common aerobic heterotrophic soil bacteria (*P. aureofaciens*) and incubated for 7 days. During the experiment, WEOM was characterised through a wide range of analytical methods (TOC, UV–Vis absorbance, high-performance ion chromatography and HRMS Orbitrap).

The results showed bacteria consumed a significantly greater proportion of WEOM produced by *C. stellaris* than by *A. polifolia* and *B. nana* at the end of the experiment ($p < 0.05$). Furthermore, the number of features in WEOM decreased for *C. stellaris* and *E. vaginatum*, whereas it increased for *B. nana*. These findings shed light on the species-specific biodegradation processes that rely on the initial composition of DOM, specifically influenced by the vegetation's capacity to produce recalcitrant compounds. Furthermore, our results emphasised that even though bacterial activity greatly impacted molecular characteristics, the WEOM produced by different vegetation species maintained their distinct molecular signatures. As a result, it can be inferred that the DOM found in natural environments directly reflects the relevant vegetation cover despite the strong influence of biogeochemical processes on DOM molecular composition. This should be considered when developing models to assess the influence of climate change on vegetation cover composition and its subsequent effects on DOM dynamics in soil and surface waters.

1. Introduction

Over the last decades, global warming has significantly impacted ecosystems and particularly the Arctic, owing to climate amplification (Serreze et al., 2009; Overland and Wang 2013; AMAP 2017). Arctic vegetation is considered highly sensitive to climate change. Multiple studies using various methods such as remote sensing, aerial photography, field experiments, and modelling have shown a long-term increase in plant cover in tundra ecosystems. This increase is accompanied by a shift towards shrubs and graminoids dominating the landscape while the abundance of lichens and bryophytes declines (Sturm et al., 2001; Tape et al., 2006; Walker et al., 2006; Myers-Smith et al., 2011; Elmendorf et al., 2012; Berner et al., 2020; Heijmans et al., 2022). On the other hand, the thawing of permafrost induced by rising temperatures enhances the formation of wetland systems and the development of

moss and graminoid-dominated ecosystems (Van Der Kolk et al., 2016; Heijmans et al., 2022).

Dissolved organic matter (DOM) is a key component of the global carbon (C) cycle. It is involved in nutrient dynamics (e.g. N, P and S) and organic and inorganic pollutant cycles such as hydrocarbons, pesticides and trace elements. DOM is also a vital substrate as it provides both C and nutrients for microbial activity in the Arctic (Kalbitz et al., 2000; Marschner and Kalbitz 2003; Mann et al., 2012; Abbott et al., 2014; Wologo et al., 2021). The environmental functions of DOM are related to its composition (Crump et al., 2003; Docherty et al., 2006; Catalán et al., 2021), which in turn depends on its source. In high-latitude surface waters, the DOM is represented by a complex mixture of vegetation leachates and biological and photochemical degradation products (Kalbitz et al., 2000; Mann et al., 2012; Ward and Cory 2016). In the Arctic, DOM biodegradation in soils mainly occurs during the short

period of spring and summer, when microbial activity is more pronounced. During several months of active (unfrozen) period, the thawing of permafrost and snowmelt leads to the export of both old and recently produced DOM from the soil to the hydrological network (Mann et al., 2015; Fouché et al., 2017). In Arctic environments, the DOM of soils and streams is anticipated to undergo reduced microbial degradation compared to regions with warmer climates (Amon et al., 2012; Fouché et al., 2017, 2020). Elevated temperatures have led to noticeable increases in terrestrial dissolved organic matter (DOM) fluxes within Arctic hydrosystems (Frey and Smith 2005; Olefeldt and Roulet 2012; Walvoord et al., 2012; O'Donnell et al., 2021). In this context, several studies have focused on characterising the DOM released from terrestrial sources, including ground vegetation (Cuss and Guéguen 2013; Hensgens et al., 2021; Allain et al., 2023) and thawing permafrost (Mann et al., 2015; Fouché et al., 2020).

In addition to DOM sources, biogeochemical processes (i.e. biodegradation, photo-oxidation and adsorption onto mineral substrates) impact DOM fluxes and composition (Kiikkilä et al., 2005; Bowen et al., 2009; Lang et al., 2009; Cuss and Guéguen 2012; Kaiser and Kalbitz 2012; Gonsior et al., 2013; Shirokova et al., 2017; Payandi-Rolland et al., 2020). A recent evaluation of DOM composition during biodegradation under various conditions revealed that the source of DOM was the most influential factor in determining the extent of microbial-induced decay (Catalán et al., 2021). However, to our knowledge, the experimental biodegradation of Arctic vegetation leachates by individual soil bacterial strain under controlled laboratory conditions, combined with the monitoring of DOM composition, has never been attempted and remains poorly constrained.

The DOM, which is the product of multiple sources and numerous biogeochemical processes, results in a complex mixture of thousands of compounds that have pushed the limits of analytical techniques used to characterise them (Nebbioso and Piccolo 2013 and references therein; Minor et al., 2014 and references therein). Therefore, a combination of several methods is almost mandatory to obtain complementary and in-depth knowledge of DOM composition (Minor et al., 2014; Rosario-Ortiz and Korak 2017). However, although different methods may provide similar information (e.g. aromaticity obtained through UV–Vis absorbance and mass spectrometry, respectively), the selectivity of each method does not always enable a straightforward comparison (Allain et al., 2023).

This work presents the results of DOM biodegradation experiments associated with a wide range of complementary analytical techniques. These experiments were focused on 1) gaining new insights on how DOM source properties influenced the early-stage biodegradation process, 2) verifying if the evolution of DOM chemical properties from different plants was similar during biodegradation, and 3) testing if specificities of DOM composition were preserved after decomposition. For this, four plants typical of Arctic environments were used as primary sources of DOM. The water extractable organic matter (WEOM) fraction was produced and incubated in the presence of a soil aerobic heterotrophic bacteria (*Pseudomonas aureofaciens*) for 7 days. During the experiment, we tracked the evolution of DOM by quantifying dissolved organic carbon, nutrients, organic acids and optical properties of DOM. Additionally, the molecular composition of WEOM was characterised through HRMS Orbitrap at the beginning and the end of the experiment.

2. Material and methods

2.1. Sampling site and sample selection

Vegetation samples were collected from a permafrost peat bog near the Khanymey Research Station (INTERACT network station, Western Siberia) and from a mire 10 km east of Abisko Research Station (INTERACT network station, Lapland, Sweden). Detailed descriptions of the sites are provided elsewhere (Johansson et al., 2011; Shirokova et al., 2013; Morgalev et al., 2017). On each site, the dominant

vegetation species were identified and selected (the lichen *Cladonia stellaris*, the graminoids *Eriophorum vaginatum*, the evergreen dwarf shrub *Andromeda polifolia* and the deciduous dwarf shrub *Betula nana*) based on their plant functional type (PFT). For each species, the fresh biomass (i.e. whole vegetation of *C. stellaris*, the stem of *E. vaginatum*, and leaves of *A. polifolia* and *B. nana*) was collected on several individuals and pooled by vegetation species and sites to form composite samples. Samples were then air-dried and kept in paper bags for further preparation.

2.2. Bulk OM properties

Each composite sample was used to characterise the chemical composition of organic matter (OM). Vegetation subsamples were ground using a rotor mill for vegetation (Ultra Centrifugal Mill ZM 200, Retsch, Haan, Germany) with a 6-tooth rotor and a 0.250 mm trapezoid holes sieve at 14,000 rpm. These ground vegetation samples were referred to as "vegetation OM" and were analysed using an elemental analyser Pyro cube EA (Elemental, Hanau, Germany), with tyrosine as the analytical standard.

2.3. WEOM extraction

For aqueous leachate preparation from each vegetation species, unground subsamples were extracted with ultra-pure water (18 MΩ cm, PURELAB® Ultra, ELGA LabWater, United Kingdom), respecting a 1/100 (w/w) ratio on a dry weight basis. Then, these mixtures and one blank of ultra-pure water were gently shaken in sterilised 500 ml bottles for 2 h on a ping-pong shaker at 20 °C. Extracts and the blank were filtered through sterilised nylon filters (0.45 μm) with sterilised filtration units to obtain the WEOM. Based on preliminary DOC analysis, some WEOM samples were diluted to obtain DOC concentrations between 20 and 72 mg_C L^{-1} for all WEOM at the beginning of the experiment. This range of DOC concentration is typical for ground depressions and small thaw ponds of studied regions (Manasypov et al., 2015). Each of the 4 diluted WEOM was then split into four 500 mL sterile glass reactors (16 reactors in total). For each vegetation species, one of the 4 WEOM samples was filtered again using a sterile filtration with a 0.22 μm nylon filter and considered as the abiotic control (see below for definition) in these experiments.

2.4. Bacterial inoculation

The soil aerobic heterotrophic gram-negative bacteria *Pseudomonas aureofaciens* (CNMN PsB-03) used in these experiments was isolated from the rhizosphere of organic-rich soils (Institute of Plant Genetics and Physiology, Moldova; see detailed description in González et al., 2014). This strain has been extensively used in several previous studies of bacterial degradation of natural DOM (Shirokova et al., 2017; Oleinikova et al., 2018). During the 4 days preceding the inoculation, *P. aureofaciens* was cultured in a sucrose-peptone broth (SP, 40 g L^{-1} sucrose, 15 g L^{-1} peptone, 5 g L^{-1} NaCl and 1.3 g L^{-1} Na_2HPO_4) for biomass accumulation at 25 °C, then harvested at the beginning of the stationary phase and centrifuged (5 min at 7000 g) to collect the concentrated biomass. At this point, aliquots of the sterilised and inoculated SP broth were sampled for further analysis. Bacteria were then starved for 24 h in a sterile NaCl (8.5 g L^{-1}) solution to remove nutrient resources. Immediately before the inoculation of reactors, bacteria were successively rinsed with sterile NaCl solution (8.5 g L^{-1}), centrifuged (5 min at 7000 g), then rinsed with ultra-pure water and centrifuged again (5 min at 7000 g) to remove any remaining elements from the cultural broth adsorbed on cell surfaces. For each vegetation WEOM, a homogeneous fraction of the bacterial suspension was added to 0.45 μm filtered WEOM to obtain initial bacterial biomass of 1g_{wet} L^{-1}. Thus, 2 reactors were inoculated for each vegetation species, and 2 additional reactors were without *P. aureofaciens* biomass and used as bacteria-free

organic-substrate controls filtered through 0.22 and 0.45 μm ($BFC_{0.22}$ and $BFC_{0.45}$, respectively; SM 1). $BFC_{0.22}$ reactors were supposed to include no bacteria (although some virus and fungus spores initially present in dry biomass could have passed through the filter), whereas $BFC_{0.45}$ reactors could contain a part of the native biomass community present on the initial vegetation samples. Reactors (inoculated and controls) were placed under dark, aerated and thermostated (20 °C) conditions on ping-pong shakers for incubation.

2.5. Aliquot sampling during the incubation

The incubation ran for 7 days, corresponding to the time required to reach stable DOC concentration in the inoculated systems. Every day, after vigorously shaking reactors for homogenisation, an aliquot of each suspension was collected for analysis. A non-filtered aliquot was used to measure specific conductivity (SC), pH and biological parameters; another aliquot was filtered through a 0.45-μm nylon syringe filter to measure UV and visible absorbance, dissolved organic carbon (DOC), dissolved nitrogen (DN), ammonia (NH_4^+), nitrate (NO_3^-), nitrite (NO_2^-) and organic acids, and to proceed to HRMS Orbitrap analysis (SM 2).

2.6. Biological parameters monitored during the incubation

Bacterial number counting was performed on days 0, 1, 2, 4, and 7 using the colony forming unit technique (CFU in cells mL^{-1}). A known volume (0.1–0.5 mL) of the non-filtered aliquots was inoculated in triplicates on nutrient agar (2.8 %) in Petri dishes. Additionally, for the inoculated reactors only, a non-filtered aliquot was inoculated in triplicates on Petri dishes using SP-based agar, allowing the specific development of *P. aureofaciens*. Inoculation of blanks (i.e. ultra-pure water) was routinely performed to ensure the absence of contamination from the external environment. Once inoculated, Petri dishes were stored in an aerated dark room, and after 5 days, CFU were manually counted. Before counting the bacteria, each colony was visually inspected to confirm it matched the morphology properties of *P. aureofaciens* colonies, as other microorganisms may also develop on SP media. The live cell concentrations of $BFC_{0.22}$ and $BFC_{0.45}$ were presented in SM 3.

2.7. Leachates geochemical characterisation

Unless explicitly stated, the sampling for analysis was performed daily.

A first set of filtered aliquots was stabilised with 3 % (v/v) HCl (reagent grade) to suppress microbial activity and stored in the refrigerator until DOC analysis. Another portion of the aliquots was immediately frozen at −20 °C for DN analysis. DOC and DN, determined as non-purgeable organic carbon (NPOC) and total nitrogen (TN), respectively, were assessed using a TOC-L analyser (Shimadzu, Kyoto, Japan). Based on the analysis of 10 blanks (i.e. fresh ultra-pure water of the day), the limits of detection (LOD) and quantification (LOQ) were 0.14 mg L^{-1} and 0.24 mg L^{-1}, respectively, for NPOC and 0.03 mg L^{-1} and 0.07 mg L^{-1}, for TN. Carbon (25 mg$_{OC}$ L^{-1}, Sigma-Aldrich, Saint Louis, Missouri, United States) and Nitrogen (1 mg$_N$ L^{-1}, Merck Group, Darmstadt, Germany) standards were used as references.

A second set of filtered aliquots was frozen at −20 °C to analyse NH_4^+, NO_3^- and NO_2^-. These compounds were quantified using a Gallery™ photometric analyser (Thermo Fisher Scientific, United States). NO_3^- and NO_2^- concentrations were assessed on days 0, 2, 4 and 7.

A third set of the filtered aliquots was frozen at −20 °C before organic acid analysis. Samples were analysed using a Dionex ICS-5000$^+$ high-performance ion chromatography with a Dionex IonPac AS11-HC column (Thermo Fisher Scientific, United States). Ion chromatography enabled the quantification of the following organic acids (LOQ = 0.002 mg$_C$ L^{-1}): 5-keto-gluconic acid ($C_6H_{10}O_7$), acetic acid ($C_2H_4O_2$), α-keto-glutaric acid ($C_5H_6O_5$), butyric acid and 2-keto-gluconic acid ($C_4H_8O_2$ and $C_6H_{10}O_7$ respectively), citric acid ($C_6H_8O_7$), formic acid (CH_2O_2),

fumaric acid ($C_4H_4O_4$), galacturonic acid ($C_6H_{10}O_7$), glutaric acid ($C_5H_8O_4$), isobutyric acid ($C_4H_8O_2$), lactic acid ($C_3H_6O_3$), maleic acid ($C_4H_4O_4$), oxalic acid ($C_2H_2O_4$), propionic acid ($C_3H_6O_2$), pyruvic acid ($C_3H_4O_3$), quinic acid ($C_7H_{12}O_6$), tartaric acid ($C_4H_4O_6$) and valeric acid, ($C_5H_{10}O_2$).

Immediately after aliquot filtration, absorbance spectra were acquired using a Cary 50 spectrophotometer (Varian, United States) with a 10 mm quartz cuvette. Scan ranged from 200 to 800 nm (interval = 1 nm at 1200 nm min^{-1}). When necessary, samples were diluted between 10 and 100 times with ultra-pure water to reach a maximum absorbance intensity of 0.1 at 254 nm to avoid the inner filter effect.

At the beginning and end of the experiment (i.e. days 0 and 7), HRMS Orbitrap analyses were performed on filtered aliquots. Sterilised SP medium and SP medium inoculated with *P. aureofaciens* (SP + *P. aureofaciens*) used to cultivate biomass before the experiment were also analysed through HRMS Orbitrap. Aliquots were stabilised with 10 % (v/v) methanol (LCMS grade) right after sampling to avoid microbial degradation of WEOM pending analysis (50 % v/v for SP and SP + *P. aureofaciens* samples). The strata-X cartridges (500 mg of sorbent, Phenomenex Inc., United States) were used for solid phase extraction (SPE) to concentrate and purify WEOM samples and to remove inorganic salts that would interfere with the electrospray HRMS Orbitrap analysis (Maria et al., 2019). Before their use, SPE cartridges were conditioned with the consecutive application of 3 mL isopropanol, 6 mL acetonitrile, 6 mL methanol (0.1 % formic acid) and 6 mL ultra-pure water (0.1 % formic acid). The sample pH was adjusted to 4.5 with concentrated formic acid. Then, approximately 10 mL of the sample was applied to the cartridges at 1 mL min^{-1}. The cartridges were then rinsed with 4 mL ultra-pure acidified water (0.1 % formic acid) to remove the inorganic salts. Cartridges were subsequently dried for 5 min, and the analytes were eluted with 2.0 mL of acetonitrile/methanol/water (45/45/10) at pH 10.4, diluted 50/50 (v/v) (10/90 v/v for SP and SP + *P. aureofaciens* samples) with ultra-pure water and analysed right away. Because low molecular weight compounds (<100 Da) were expected to be lost in the rinsing and drying steps of the SPE (Zhao et al., 2013), HRMS samples were here designated as $WEOM_{SPE}$. The eluted $WEOM_{SPE}$ samples were then infused into an ESI(−) source with an LTQ-Orbitrap XL mass spectrometer (Thermo Scientific, San Jose, CA, USA). Solvent blanks were run before and after each sample to clean up the ion source and avoid cross-contamination between samples.

2.8. Data processing and statistical analysis

2.8.1. Biological parameters

For inoculated reactors, the CFU counted on SP-based agar corresponded to the *P. aureofaciens* strain. In contrast, the CFU counted on the nutrient agar were considered as representative of cultivable native microbial consortia. The microbial data for the inoculated reactors presented here corresponded to the average number of live cells in the 2 replicates.

2.8.2. Variations of dissolved organic carbon and dissolved nitrogen

Comparisons of general variations in DOC concentration were made using the value relative to the initial DOC concentrations, calculated as follows:

$$DOC_{RIC} = \frac{DOC_{t=x} - DOC_{t=0}}{DOC_{t=0}} \times 100 \tag{1}$$

With "DOC_{RIC}" (in %$DOC_{t=0}$) the DOC variation, relative to the initial DOC concentration, "$DOC_{t=x}$" the concentration (mg L^{-1}) at a given time "x" (days) and $DOC_{t=0}$ the concentration at the beginning of the experiment. It has to be noted that the DOC_{RIC} corresponds to net values, i.e. the balance between gains and losses relative to the initial values. According to this equation, a positive DOC_{RIC} indicates a DOC increase, meaning a net DOC production, whereas a negative DOC_{RIC} indicates a

DOC decrease, meaning a net DOC consumption.

The measured NH_4^+, NO_2^- and NO_3^- concentrations (in mg L^{-1}) were converted into N–NH$_4^+$, N–NO$_2^-$, N–NO$_3^-$ (in mg$_N$ L^{-1}) respectively, and organic N (N$_{org}$ in mg$_N$ L^{-1}) was calculated by subtracting N–NH$_4^+$, N–NO$_2^-$ and N–NO$_3^-$ to TN.

2.8.3. Absorbance indices

Based on absorbance analysis, specific ultraviolet absorbance at 254 nm (SUVA$_{254}$) and absorbance ratios at 254 nm–356 nm (E2/E3) were calculated to characterise WEOM. SUVA$_{254}$ is related to DOM aromaticity (Weishaar et al., 2003; Peacock et al., 2014), with high values of SUVA$_{254}$ (in L mg$_C^{-1}$ m^{-1}) indicating a more aromatic DOM. The E2/E3 index is a proxy of DOM molecular weight (MW, Hunt and Ohno, 2007), with lower E2/E3 indicating higher MW of DOM and conversely.

2.8.4. Organic acids

The concentrations of organic acids were summed for each reactor and time step and referred to as "organic acids". When necessary, missing data were approximated by averaging the values of the previous and the next day.

2.8.5. HRMS orbitrap data processing

The data acquisition and recalibration were done using the Thermo Xcalibur software. The eluted WEOM$_{SPE}$ samples were infused into an ESI(−) source with a spray voltage of 3.5 kV at a flow rate of 15 μL min-1. Data were acquired in the mass range of 50–1000 m/z. At least 50 scans of each sample were averaged to get an individual spectrum (see Maria et al., 2019 for more details on the method). Mass accuracy was checked by inspecting the attribution of the elemental composition of phthalates and PDMS (known background compounds). The post-acquisition recalibration was based on a 5-order polynomial equation, using a set of naturally occurring compounds (lignins and natural organic matter) selected to represent internal recalibrants in the considered mass range (50–800 m/z). The recalibration was validated by checking that the average errors to the reference masses were lower than 0.5. After background ion removal, the elemental compositions were assigned with an error lower than 3 ppm. The elemental compositions were assigned, respecting the user-defined C$_{1–70}$H$_{0–140}$O$_{1–25}$N$_{0-4}$ composition and were validated by checking the error distribution, which had to be between −1 and 1 ppm and equitably distributed around 0 ppm. Since the ionisation yield might differ between molecules, the high-resolution data were only considered to compare the number and distribution among biomolecule families of identified formulas in the different WEOM$_{SPE}$ species. Then, based on the information provided by the HRMS Orbitrap, the double bond equivalent (DBE$_{AI}$) and aromaticity index (AI) were calculated to get insight into the degree of unsaturation and aromaticity in a molecule (Koch and Dittmar 2006; Maria et al., 2019).

2.8.6. Visual representation of HRMS orbitrap data

Van Krevelen (VK) diagrams concisely present complex information obtained from HRMS Orbitrap by displaying the elemental ratios (O/C vs H/C) for each assigned formula. By analysing the positioning of these formulas within the VK diagram, valuable insights can be gained regarding the formulas and their distribution among various biomolecule families. These families include lipid-like, protein-like, amino sugar-like, carbohydrate-like, condensed hydrocarbons, lignin-like, tannin-like, and aromatic structures (SM 4). The abundance of assigned formulas belonging to each biomolecule family can be determined using Van Krevelen diagrams. Furthermore, the assigned molecular formulas can be categorised into different classes based on their composition, such as C and H-containing formulas (CH), C, H, and O-containing formulas (CHO), and C, H, O, and N-containing formulas (CHON). Venn diagrams were used to compare the molecular composition of multiple samples, illustrating the overlapping and unique components among the samples.

By examining the molecular compositions of different plant species, it was possible to identify the shared and distinctive formulas associated with each species. Analysing the changes in molecular composition from the initial to the final stages revealed features generated and consumed during the biodegradation of WEOM. Similarly, comparing the molecular composition of the sterile SP medium with that of the SP medium supplemented with *P. aureofaciens* allowed for inferences regarding the molecular composition of *P. aureofaciens*. The proportion of bacterially-derived features to the total features was used to estimate the bacterial influence on the molecular composition of WEOM$_{SPE}$ for a given vegetation species (SM 5).

To facilitate the analysis of changes in the molecular compositions of the samples, the relative enrichment factor was computed for each biomolecule family and vegetation species using the following formula:

$$EF_{family} = p_{final} - p_{initial} \qquad (2)$$

with EF$_{family}$ (%) a relative enrichment factor, p the proportion (%) of detected formulas belonging to a biomolecule family at the beginning ("initial") or at the end ("final") of the experiment.

2.8.7. Statistical analysis

Statistical analyses were performed using R 3.6.1 (The R Foundation for Statistical Computing, Austria) and RStudio 1.2.1335 (RStudio Inc., MA, USA). Statistical analyses were systematically applied to all the chemical metrics. Statistical significance was tested using the non-parametric Mann-Whitney test (α = 0.05) to compare medians measured at the beginning and end of the experiment. Additionally, statistical significance was tested using the non-parametric Kruskall-Wallis test (α = 0.05) with a posthoc Dunn test (α = 0.05) using the "dunn.test" package (Dinno 2017) to compare medians of measured variables of the 4 vegetation species either at the beginning or at the end of the experiment. The results of the statistics were synthesised in SM 6.

3. Results

3.1. Microbial biomass evolution during the experiment

The initial *P. aureofaciens* live cell concentrations ranged between 1.3 (±0.4) × 10^7 and 2.1 (±0.3) × 10^7 CFU mL^{-1}, representing 100 % of the total heterotrophic cultivable live cells (Fig. 1). Then, the *P. aureofaciens* concentration increased until day 2 (*B. nana*) or day 4 (*C. stellaris, E. vaginatum, A. polifolia*), and reached between 8.1 (±0.3) × 10^7 and 2.0 (±0.7) × 10^8 CFU mL^{-1} (85–88 % of the total heterotrophic cultivable live cells), then decreased to reach 7.1 × 10^7 to 1.0 (±0.1) × 10^8 CFU mL^{-1} (between 47 and 53 % of the total heterotrophic cultivable live cells). Between the beginning and the end of the experiment, the *P. aureofaciens* live cell concentration increased by a factor of 3–5.

3.2. Consumption of DOC and production of DN

The initial DOC concentrations were significantly (p-value <0.05) greater for *B. nana* compared to *E. vaginatum* with 72.4 ± 0.0 and 18.9 ± 2.2 mg$_C$ L^{-1} respectively, and the DOC concentration of *C. stellaris* and *A. polifolia* were 24.9 ± 0.8, 45.5 ± 1.4 mg$_C$ L^{-1} respectively (SM 7). A significantly greater amount of the DOC was consumed after 7 days of incubation *C. stellaris* compared to *B. nana* and *A. polifolia* (−70 ± 2, −36 ± 4 and −39 ± 5 %DOC$_{t=0}$ respectively; p-value <0.05), with a maximal consumption in the first two days of the experiment (Fig. 2 and SM 7 and 8).

The initial TN of inoculated WEOM was significantly (p-value <0.05) greater for *C. stellaris* than *E. vaginatum*, with 1.99 ± 0.21 and 0.41 ± 0.02 mg$_N$ L^{-1}, respectively (SM 9). During the experiment, the TN significantly increased (p-value = 0.001). This was particularly noticeable for *A. polifolia* and *E. vaginatum* (multiplied by 6 and 11, respectively). No$_2^-$ or NO$_3^-$ was detected during the experiment except for one
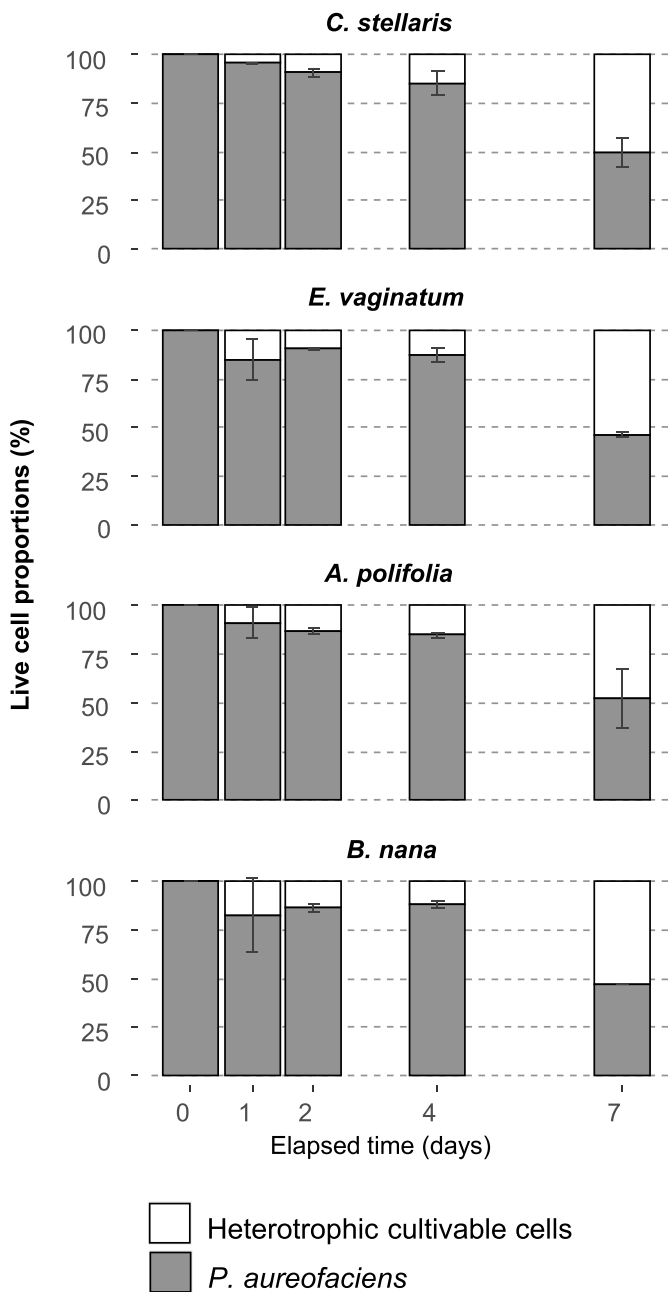
Fig. 1. Evolution of the live cell proportions of (top to bottom) *C. stellaris*, *E. vaginatum*, *A. polifolia* and *B. nana* inoculated WEOM (% CFU). White bars correspond to heterotrophic cultivable cells, and dark grey bars correspond to *P. aureofaciens* (%).

Fig. 2. Variations of DOC_{RIC} ($\%DOC_{t=0}$) during biodegradation of *C. stellaris* (purple circles), *E. vaginatum* (dark blue squares), *A. polifolia* (light blue diamonds) and *B. nana* (green triangles). Values correspond to the mean value of the replicates (n = 2) and error bars correspond to the standard deviation of inoculated WEOM replicates (n = 2). Letters (a, ab and b) correspond to the statistical difference between species at day 7.
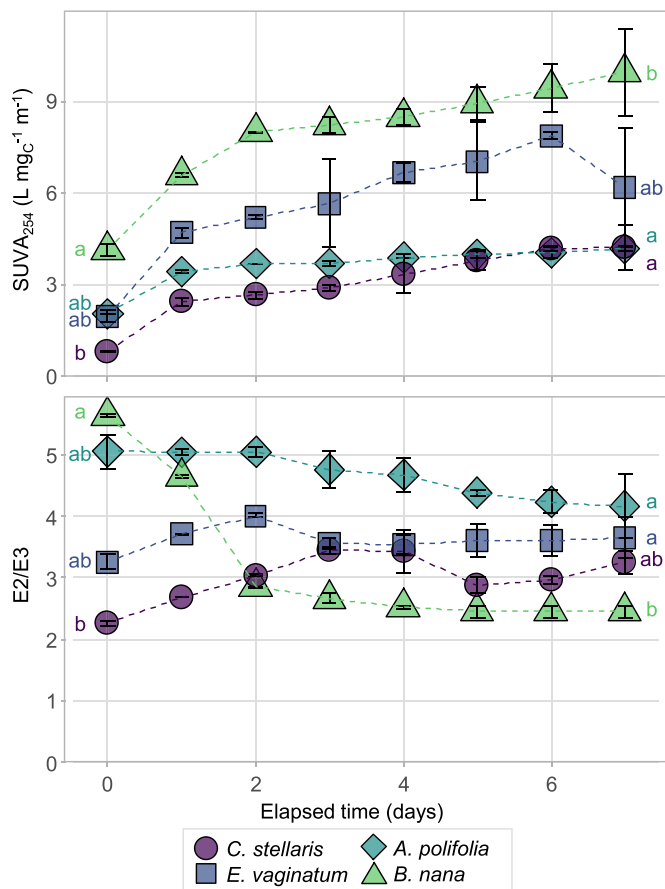
Fig. 3. Variation of (top) aromaticity ($SUVA_{254}$ in L mg_C^{-1} m^{-1}), and (bottom) molecular weight (E2/E3) during biodegradation of *C. stellaris* (purple circles), *E. vaginatum* (dark blue squares), *A. polifolia* (light blue diamonds) and *B. nana* (green triangles). Values correspond to the mean value of inoculated WEOM replicates (n = 2) and error bars correspond to the standard deviation of inoculated WEOM replicates (n = 2). Letters (a, ab and b) correspond to the statistical difference between species at day 0 and 7 respectively.

replicate of *E. vaginatum* and *A. polifolia* initial inoculated reactor. The initial NH_4^+ represented 25 ± 1 and 15 % of the TN (the remaining fraction being N_{org}) for *C. stellaris* and *E. vaginatum*, respectively, but was negligible for *A. polifolia* and *B. nana*. During the experiment, the NH_4^+ fraction significantly increased (p-value = 0.017) up to 72 ± 20 % of the TN, with more substantial increases observed for *E. vaginatum* and *A. polifolia* compared to *C. stellaris* and *B. nana*.

3.3. Optical proxies of DOM

At the beginning of the experiment, the aromaticity ($SUVA_{254}$) was more important for *B. nana* (4.1 ± 0.2 L mg_C^{-1} m^{-1}) compared to *C. stellaris* WEOM (0.8 ± 0.0 L mg_C^{-1} m^{-1}; Fig. 3, SM 8). The aromaticity of all WEOM significantly increased (p-value = 0.001) with time and

reached 4.2 ± 0.1 L mg_C^{-1} m^{-1} to 10.0 ± 1.4 L mg_C^{-1} m^{-1}. At the end of the experiment, the aromaticity of *B. nana* was significantly (p-value <0.05) greater than *C. stellaris* and *E. vaginatum* ($SUVA_{254}$ of 4.2 ± 0.7 and 6.2 ± 2.0 L mg_C^{-1} m^{-1}, respectively).

At the beginning of the experiment, the molecular weight proxy E2/E3 ranged between 2.3 ± 0.0 for *C. stellaris* and 5.6 ± 0.0 for *B. nana*. (Fig. 3, SM 8). An increase of the E2/E3, corresponding to a decrease of the molecular weight, was observed for *C. stellaris* (3.2 ± 0.2) and *E. vaginatum* (3.6 ± 0.3) WEOM. In contrast, the molecular weight increased for *A. polifolia* (4.2 ± 0.5) and *B. nana* (2.4 ± 0.1).

3.4. Organic acids

At the beginning of the experiment, the proportions of DOC in organic acid form were similar (p-value >0.05) for all vegetation species and varied between 10 ± 2 and 20 ± 2 % DOC. A significant consumption (p-value $= 0.028$) of the organic acids was observed in the first days of the experiment. At the end of the experiment, organic acids only represented 1 ± 0 to 4 ± 3 % of the DOC, except for *A. polifolia* (16 ± 5 % DOC).

3.5. Molecular composition of WEOM

3.5.1. Molecular composition of initial WEOM_SPE

At the beginning of the experiment, 525, 531, 860 and 763 individual molecular formulas were assigned in *C. stellaris*, *E. vaginatum*, *A. polifolia* and *B. nana* $WEOM_{SPE}$, respectively (SM 10). The CHO and CHON formula classes represented 85–93 % and 5–14 % of assigned formulas in all $WEOM_{SPE}$, respectively. The distribution of formulas in the VK diagram showed similarities between *C. stellaris* and *E. vaginatum*, with approximately 63 % of the formulas categorised as lignin-like, 11 % as lipid-like, around 10 % as protein-like, and 8 % as aromatic structures (SM 10). In contrast, *A. polifolia* $WEOM_{SPE}$ had 52 % lignin-like formulas, 13 % lipid-like formulas, 18 % protein-like formulas, and a combined 10 % of aromatic and tannin-like formulas. Lastly, *B. nana* $WEOM_{SPE}$ consisted of 53 % lignin-like formulas, 9 % lipid-like formulas, 18 % protein-like formulas, 9 % aromatic structures, and 6 % tannin-like formulas. At last, by comparing the distinctive features of $WEOM_{SPE}$, it was possible to identify vegetation WEOM-specific formulas at the onset of the experiment (Fig. 5). None of the molecular formulas of $WEOM_{SPE}$ were exclusive to *C. stellaris* or *E. vaginatum*. However, 212 formulas were specific to *A. polifolia* $WEOM_{SPE}$ and 117 specific to *B. nana* $WEOM_{SPE}$, accounting for 25 % and 15 % of the formulas in these respective samples. Moreover, 420 formulas were found to be shared among all vegetation species in $WEOM_{SPE}$ (Fig. 5).

3.5.2. Molecular composition of WEOM_SPE after 7 days of biodegradation

At the end of the incubation, 142, 168, 733 and 1786 formulas were attributed in *C. stellaris*, *E. vaginatum*, *A. polifolia*, and *B. nana* inoculated $WEOM_{SPE}$ respectively, with 90–100 % belonging to the CHO class (SM 11). The $WEOM_{SPE}$ were composed of 44–57 % of lignin-like formulas, 10–32 % of lipid-like formulas, and 14–23 % of protein-like formulas. The tannin-like and aromatic formulas represented less than 8 % of the formulas, whereas unsaturated HC, amino-sugar-like, and carbohydrates represented less than 5 %. At the end of the experiment, 10, 3, 54 and 1121 formulas were specific to the inoculated $WEOM_{SPE}$ of *C. stellaris*, *E. vaginatum*, *A. polifolia* and *B. nana*, respectively (Fig. 5). This represented 7, 2, 7 and 63 % of the formula in *C. stellaris*, *E. vaginatum*, *A. polifolia* and *B. nana* $WEOM_{SPE}$ respectively.

3.5.3. Evolution of the WEOM_SPE molecular composition

Enrichment factors allowed for the evaluation of changes in the distribution of $WEOM_{SPE}$ molecules across different biomolecule families. During $WEOM_{SPE}$ biodegradation, the percentage of lipid-like formulas increased by approximately 2–20 % across all vegetation species (Fig. 6). Similarly, the percentage of protein-like formulas increased

by about 3–10 % for all species, except for *A. polifolia* $WEOM_{SPE}$, where there was a decrease of 2 % in the proportion of protein-like formulas. When considering all vegetation species, the proportion of lignin-like and aromatic formulas decreased by 1–20 % and 1–7 %, respectively. The proportion of tannin-like formulas remained unchanged (<2 %) during incubation. Furthermore, the number of formulas classified as amino sugar-like, carbohydrates, and unsaturated hydrocarbons was not significant for most species. Therefore, these formula classes were not further represented nor discussed.

3.5.4. Influence of P. aureofaciens on WEOM_SPE molecular composition

HRMS Orbitrap analysis allowed for the assignment of 574 formulas in the *P. aureofaciens* sample. Among these formulas, approximately 69 % were attributed to dissolved organic nitrogen formulas (CHON), whereas about 29 % were attributed to formulas containing only oxygen and hydrogen (CHO) (refer to SM 10). In the VK diagram, approximately 47 % of the assigned formulas were classified as lignin-like formulas, whereas 47 % were attributed to a combination of lipid-like, protein-like, and unsaturated hydrocarbon formulas. Around 6 % of the formulas were also assigned to amino sugar-like, carbohydrates, tannin-like, and aromatic structured formulas (SM 10).

At the beginning of the experiment, the bacterially-derived features represented 18–25 % of the $WEOM_{SPE}$ total features (SM 5). After 7 days of incubation, it represented 57, 42 and 19 % of the features detected in *C. stellaris*, *E. vaginatum* and *A. polifolia* respectively, and only 9 % of *B. nana* $WEOM_{SPE}$ formulas. The formulas attributed in both vegetation species and *P. aureofaciens* $WEOM_{SPE}$ were mainly attributed to lignin-like, lipid-like, and protein-like formulas. Few formulas were attributed to amino sugar-like, carbohydrates, and tannin-like formulas, and no formula was attributed to unsaturated HC or aromatic structures (Fig. 7).

4. Discussion

4.1. Evolution of DOM properties among vegetation species

This study provided evidence that irrespective of the vegetation type, the degradation of DOM exhibited consistent patterns for most DOM parameters. Specifically, both DOC and organic acids were consumed. In contrast, the aromaticity and TN content increased for the WEOM derived from the four vegetation species. However, the changes in DOM molecular weight and molecular composition varied depending on the specific vegetation type. Additionally, the aromaticity, molecular weight and molecular properties highlighted the differences in WEOM compositions among vegetation species at the end of the experiments (Figs. 3, 5 and 6). Indeed, the aromaticity of *E. vaginatum* and *B. nana* leachates were higher than those of *C. stellaris* and *A. polifolia*. Additionally, the analysis of molecular properties revealed contrasting trends in the number of formulas during the biodegradation process. Specifically, the number of formulas decreased for *C. stellaris* and *E. vaginatum* $WEOM_{SPE}$ in accordance with the literature (Hensgens et al., 2021). In contrast, it increased for *A. polifolia* and *B. nana* $WEOM_{SPE}$ (Figs. 5 and 6, and SM 10 and 11). Also, in the presence of *P. aureofaciens*, the proportion of common formulas increased for *C. stellaris*, *E. vaginatum* and *A. polifolia* in accordance with Brock et al. (2020) but decreased for *B. nana* $WEOM_{SPE}$ (Fig. 6).

These findings provide insights into the potential processes that govern the biodegradation of WEOM from different vegetation species. Specifically, the degradation of *B. nana* WEOM involved the mineralisation of LMW compounds, resulting in a DOM with a higher molecular weight than its fresh equivalent (Fig. 3). In contrast, the degradation of WEOM from *C. stellaris*, *E. vaginatum*, and *A. polifolia* resulted in the mineralisation of low molecular weight (LMW) compounds (Fig. 4). Finally, the molecular properties of the $WEOM_{SPE}$ from different vegetation species underscored the retention of their unique characteristics (Figs. 5 and 6) despite substantial degradation of DOC (Fig. 2). The
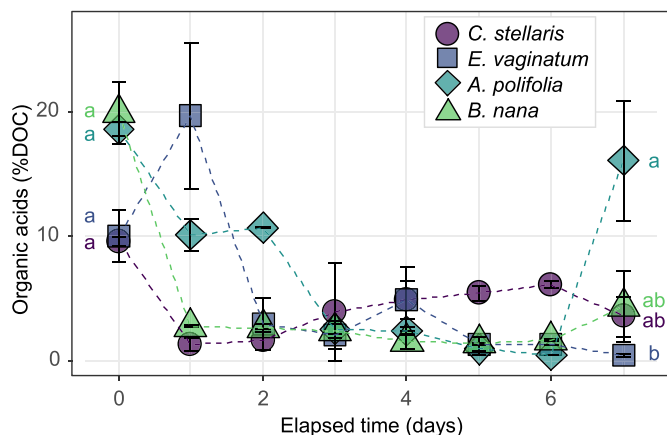
Fig. 4. Consumption of organic acid (% DOC) during biodegradation of *C. stellaris* (purple circles), *E. vaginatum* (dark blue squares), *A. polifolia* (light blue diamonds) and *B. nana* (green triangles). Values correspond to the mean value of inoculated WEOM replicates (n = 2) and error bars correspond to the standard deviation of inoculated WEOM replicates (n = 2). Letters (a, ab and b) correspond to the statistical difference between species at day 0 and 7 respectively.

number of formulas in the WEOM varied across the species, with only a few formulas detected in *C. stellaris* and *E. vaginatum*, whereas a considerably larger number of 1121 formulas were identified in *B. nana* (Figs. 5 and 6 and SM 11). The vegetation leachates were expected to display more tannin-like carbohydrates and aromatic structures and less lipid-like and protein-like formulas (Kögel-Knabner, 2002) than they actually do. However, these molecular compositions were in line with the reported litter leachate composition (Brock et al., 2020) that exhibited a significant abundance of lignin-like formulas and a limited abundance of condensed HC and aromatic structures (Fig. 5). These results could be attributed to the ionisation yield that differs between compounds (Nebbioso and Piccolo 2013), to the misleading nomination of biomolecule families (e.g. the use of compound-"like" nomination) or to the bacterial influence on molecular composition (Fig. 8).

The rapid decline in DOC observed in the bacteria-inoculated re-actors was attributed to using easily degradable compounds, including organic acids, amino sugar-like formulas, and carbohydrates (Figs. 2, 4 and 7). This substantial consumption of DOC occurred predominantly within the initial 2–3 days of the experiment. (Figs. 2 and 4). These results are consistent with the previously reported preferential use of labile organic acids by microorganisms (Van Hees et al., 2002) and with their typical half-life in soil of 0.5–12 h (Jones et al., 2001; Van Hees et al., 2005 and references therein). It is important to note that the *C. stellaris* and *E. vaginatum* inoculated reactors exhibited a higher pro-portion of labile compounds compared to the *A. polifolia* or *B. nana* re-actors. This is evident from the greater losses of dissolved organic carbon (DOC) observed after 2 days in the former reactors (Fig. 2). On the other hand, the slight decrease of DOC observed after the third day of the experiment was attributed to the degradation and consumption of less bioavailable compounds. This preferential consumption of labile com-pounds, which corresponded to UV-inactive DOM (Marschner and Kal-bitz 2003), resulted in a relative increase of the less bioavailable (or "slowly degradable") compounds. This shift was illustrated by an in-crease in WEOM aromaticity (Fig. 3). The preferential biodegradation of small labile compounds also resulted in an increase in *B. nana* molecular weight, as illustrated by a decrease in the E2/E3 index (Fig. 3). Overall, this may reflect a relative increase in high molecular weight compounds (e.g. lignin, cellulose and hemicellulose) at the expense of more labile, LMW compounds, and an increase in the detectable pool of higher molecular weight molecules. These conclusions were made based on the aromaticity index obtained through absorbance data (Fig. 3). It has to be noted that the aromaticity indices $SUVA_{254}$ and AI calculated based on
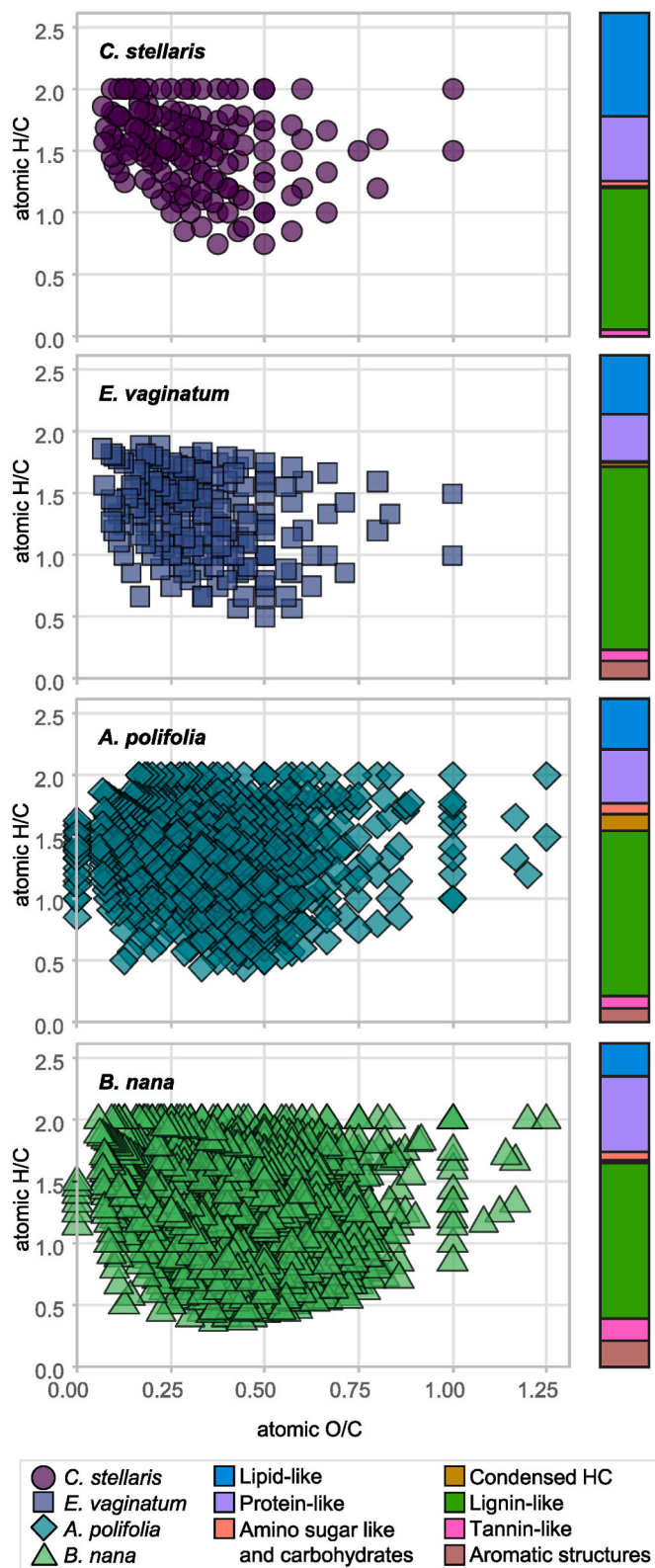
Fig. 5. Van Krevelen diagrams (left) and distribution of formulas among biomolecule families (right) of (top to bottom) *C. stellaris* (purple circles), *E. vaginatum* (dark blue squares), *A. polifolia* (light blue diamonds) and *B. nana* (green triangles) inoculated WEOM at the end of the incubation experiment. Each symbol of the Van Krevelen diagrams represent a unique formula detected in the sample.
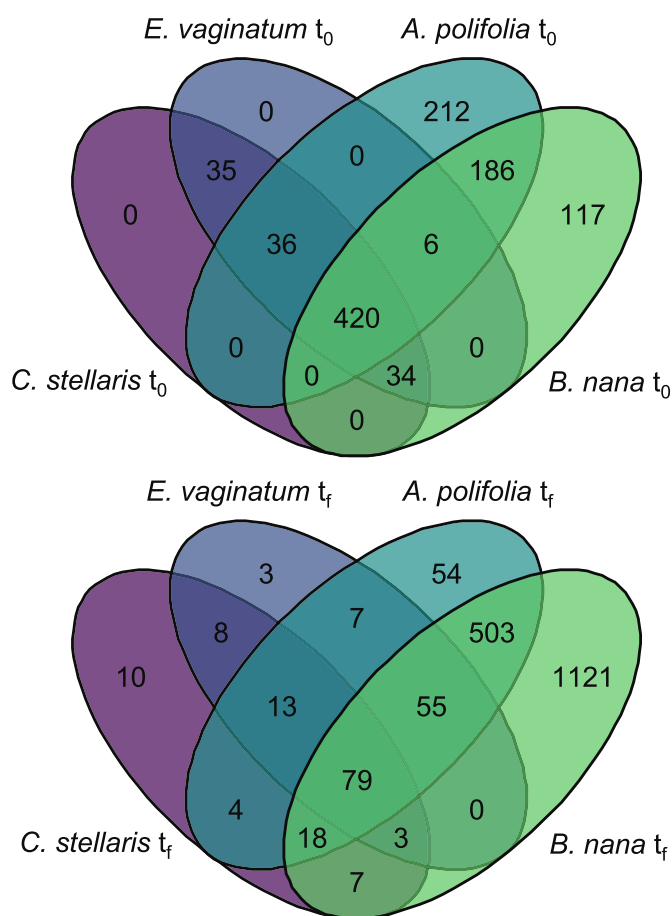
Fig. 6. Venn diagrams formulas detected in *C. stellaris* (purple), *E. vaginatum* (dark blue), *A. polifolia* (light blue) and *B. nana* (green) inoculated WEOMSPE at the beginning (up) and at the end (down) of the biodegradation experiments. The numbers correspond to the formula that are shared (overlapping regions) between 2 or more samples, or unique (non overlapping regions) to a sample.
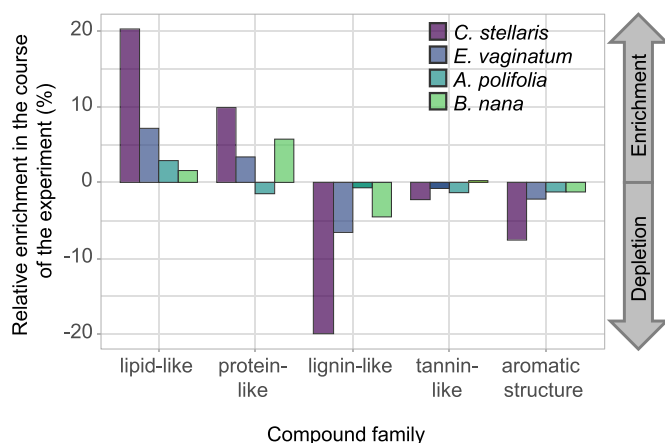
Fig. 7. Relative enrichment in each biomolecule family for *C. stellaris*, *E. vaginatum*, *A. polifolia* and *B. nana*. Positive values correspond to a relative enrichment and negative values correspond to a relative depletion for a given biomolecule family. No significant change in the relative contribution of condensed HC amino sugar-like and carbohydrate compounds was detected for any vegetation species and these biomolecule families were not represented on the figure.

absorbance and molecular analysis, respectively, do not correlate to each other (Fig. 3 and SM 10 and 11) as it was also reported in a previous study on WEOM produced by vegetation samples (Allain et al., 2023). These differences were attributed to the selectiveness of each analytical method toward different compounds. Despite these differences, the wide use of SUVA$_{254}$, the agreement between replicates, and the consistent temporal pattern observed in the experiments enable efficient use of this index.

4.2. Biological influence

Throughout the experiments, the changes in the distribution among molecular families (Fig. 5) and the increase of bacterially-derived features (Fig. 7, SM 5) demonstrated a shift in the molecular signature of inoculated WEOM$_{SPE}$ towards an evident influence of bacterial activity. These results were in line with expectations and validated the applicability of the semi-quantitative approach using HRMS Orbitrap despite its limitations as a quantitative method.

The molecular signature of *P. aureofaciens* (SM 10 and 12) displayed a stark contrast to that of the initial vegetation samples (SM 10). *P. aureofaciens* exhibited higher proportions of lipid-like, protein-like, amino-sugar, and carbohydrate formulas. This observation aligns with the known ability of *P. aureofaciens* to produce a substantial amount of extracellular polymeric substances (EPS), as documented in studies by González et al. (2010), Drozdova et al. (2014) and Oleinikova et al. (2018). These EPS primarily consist of polysaccharides, proteins, DNA, and lipids. (Wingender et al., 1999; Flemming and Wingender 2010; Costa et al., 2018). At last, the significant presence of lignin-like formulas in the molecular signature of *P. aureofaciens* may be attributed to other formula categories, such as peptides or nucleotides, as suggested by Rivas-Ubach et al. (2018). This finding is consistent with the high proportion of formulas containing carbon, hydrogen, oxygen, and nitrogen (CHON; SM 10).

4.3. Initial DOM properties drive biodegradation dynamics

Results revealed rather contrasted DOM properties after 7 days of biodegradation, depending on the initial vegetation source. Indeed, as illustrated by the DOC$_{RIC}$, the WEOM of *C. stellaris* and *E. vaginatum* was sizably more biodegradable than that of *B. nana* and *A. polifolia*. Similar DOC consumptions were reported in previous studies on vegetation leachate biodegradation (Pinsonneault et al., 2016; Shirokova et al., 2017), and the comparison of DOC$_{RIC}$ between functional types exhibited the following order: lichen $\geq$ graminoid $\geq$ (evergreen shrub = deciduous shrub). In natural settings, the differences in OM biodegradation were attributed to three categories of governing parameters, namely (1) soil properties (i.e. nutrient availability, microbial community structure and other soil solution constituents), (2) external factors (i.e. temperature, rainfall regime and vegetation cycles) and (3) intrinsic DOM characteristics such as the molecular composition, functional groups and the size of the molecules (Marschner and Kalbitz 2003; Wickland et al., 2007). Since our experiments were performed under controlled conditions in filtered water leachates, the differences in biodegradation between vegetation species should be attributed mainly to the intrinsic DOM properties. In particular, the bioavailability of DOM compounds and overall kinetics of biodegradation depend on the proportion of labile *vs* slowly degradable and biologically resistant DOM (Qualls and Haines 1992; Kalbitz et al., 2003; Marschner and Kalbitz 2003). An increase in N–NH$_4^+$ in the inoculated reactors could be attributed to the ammonification associated with the DOM decomposition by microbial biomass. It is also consistent with a pronounced bacterial biomass growth during the first days and a decrease afterwards.
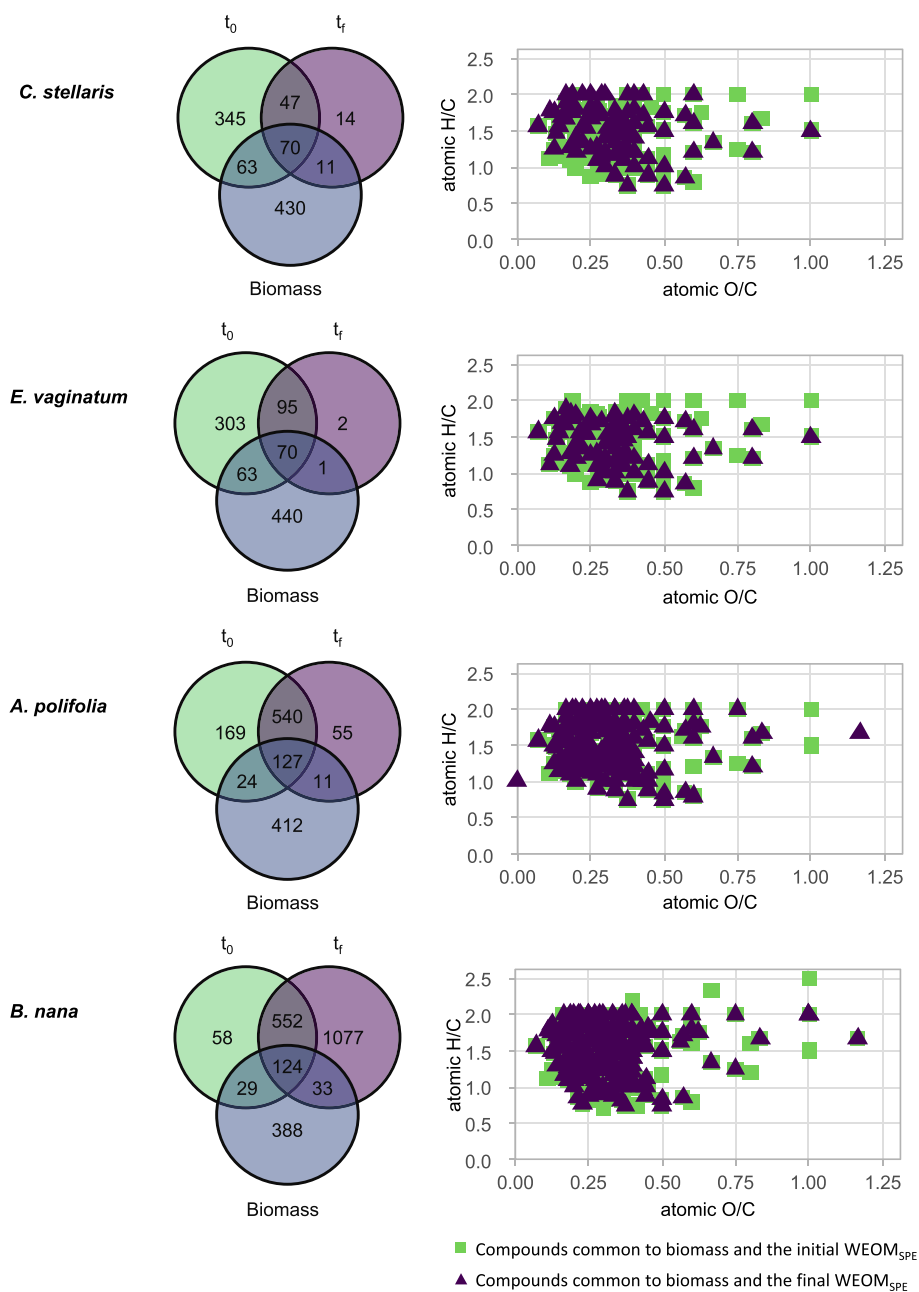
Fig. 8. Venn diagrams (left) of compounds shared between the biomass (blue), the beginning (green) and the end (purple) of the experiments for (up to down) *C. stellaris*, *E. vaginatum*, *A. polifolia* and *B. nana* WEOMSPE; associated Van Krevelen diagrams (right) of common compounds between biomass and initial WEOMSPE (green) and final WEOMSPE (purple).

4.4. Consequences for climate-sensitive arctic environments

Despite the intrinsic limitations of the experimental approach to mimic the natural processes (duration of the experiment, the sole source of DOM, restricted bacterial consortium, constant external physical parameters such as light and temperature), this study enabled characterising the processes that are challenging to observe and measure *in situ*. First, the leaching of DOM from fresh vegetation and litter rapidly enhances biological activity by bringing fresh nutrients to the soil (Kalbitz et al., 2007). The labile fraction is expected to be quickly consumed by soil microorganisms and transformed into microbial biomass or mineralised. As a result, DOM evolves along the vegetation-soil-water continuum towards more refractory compounds by suppressing the signal of the most labile compounds. However, it was reported that DOM from arctic hydrographic systems was still highly dynamic and labile (Mann

et al., 2012) despite a long transport (hence degradation) time of DOM within the soil (Speetjens et al., 2022). This finding could be partially explained by a potentially significant contribution of fresh vegetation leachates to Arctic surface waters.

The Arctic ecosystems include peatlands, lichen and moss tundra, and shrub tundra, characterised by contrasted vegetation cover. Climate change is causing tundra greening and the northward migration of tree and shrub boundaries (Sturm et al., 2001; Epstein et al., 2013). The present work demonstrates that the properties and biodegradability of WEOM are vegetation-specific, with a potential for these compounds to be preserved in the environment for a longer time thanks to the occurrence of biodegradation-resistant compounds such as waxes, tannins and aromatic molecules. Thus, ecosystems covered by contrasted vegetation are expected to provide distinct DOM signatures that closely reflect the vegetation cover composition that produced them. This opens up the

possibility of tracing the sources of DOM depending on vegetation species in different soil and aquatic environments.

Finally, Ward and Cory (2015) showed that the DOM produced by different soil horizons with different chemical compositions may not induce different bacterial respiration rates when exported to arctic rivers. Considering upstream processes, such as the leaching of fresh vegetation and litter, our results illustrate that the change of Arctic vegetation may significantly modify the microbial respiration rate of the DOM. Indeed, Catalán et al. (2021) showed the importance of DOM quality and sources for the decomposition processes. Consistently, we showed that, beyond the different environmental compartments (aquatic, soil, and vegetation), the different vegetation can produce very contrasted DOM. Currently occurring shifts in the geographical pattern of Arctic plant communities are expected to significantly affect the DOM biodegradability in the adjacent aquatic ecosystems.

Generally, the input of bio-labile DOM from vegetation has been reported to enhance the biodegradation of stable DOC in natural settings (Cleveland et al., 2007; Kalbitz et al., 2007; Crow et al., 2009). Specifically, this study shows that shrubs produce more organic acids, protein-like formulas, amino-sugar-like, and carbohydrates than lichens and graminoids. It follows that the northward migration of the treeline is likely to increase the input of DOM, whose microbially-induced degradation may enhance CO_2 emissions, biomass production, and nutrient transfer to both terrestrial and aquatic ecosystems. These retroactive relationships should be considered for modelling biogeochemical C cycling between soil and waters in high latitudes.

5. Conclusion

Based on a biodegradation experiment associating a wide range of complementary analytical techniques, we assessed the evolution of chemical properties of WEOM produced by contrasted Arctic vegetation species. The four vegetation species studied in this experiment produced WEOM with contrasted chemical properties. We revealed similar trends of DOC and organic acid consumption, whereas the evolution of qualitative properties (UV–visible, molecular signatures) were species-specific and appeared to be a function of the initial WEOM composition. This study demonstrates that the vegetation species source determined the overall biodegradation kinetics, depending on the proportion of labile vs. slowly degradable and biologically resistant WEOM. Furthermore, after 7 days of the biodegradation experiment, despite showing a strong microbially produced signature, WEOM still exhibited vegetation-specific molecular properties. Therefore, WEOM extracted from contrasted vegetation species is capable of preserving its specific properties after biodegradation. These conclusions are important for DOM dynamics since the DOM produced by contrasted and changing Arctic ecosystems may significantly change in the forthcoming years.

CRediT authorship contribution statement

Alienor Allain: Writing – review & editing, Writing – original draft, Visualization, Investigation, Formal analysis, Data curation, Conceptualization. **Marie A. Alexis:** Writing – review & editing, Writing – original draft, Supervision, Investigation, Funding acquisition, Conceptualization. **Maxime C. Bridoux:** Writing – review & editing, Writing – original draft, Investigation, Formal analysis, Data curation. **Liudmila S. Shirokova:** Writing – review & editing, Writing – original draft, Investigation, Data curation, Conceptualization. **Dahédrey Payandi-Rolland:** Writing – review & editing, Writing – original draft, Investigation, Formal analysis, Data curation, Conceptualization. **Oleg S. Pokrovsky:** Writing – review & editing, Writing – original draft, Investigation, Conceptualization. **Maryse Rouelle:** Writing – review & editing, Writing – original draft, Supervision, Investigation, Funding acquisition, Conceptualization.

Declaration of competing interest

The authors declare that they have no known competing financial interests or personal relationships that could have appeared to influence the work reported in this paper.

Data availability

Data will be made available on request.

Appendix A. Supplementary data

Supplementary data to this article can be found online at https://doi.org/10.1016/j.soilbio.2024.109393.

References

Abbott, B.W., Larouche, J.R., Jones, J.J.B., et al., 2014. Elevated dissolved organic carbon biodegradability from Thawing and Collapsing Permafrost. J Geophys Res Biogeosciences 119, 2049–2063. https://doi.org/10.1002/2014JG002678.Received.

Allain, A., Alexis, M.A., Bridoux, M.C., et al., 2023. Fingerprinting the elemental composition and chemodiversity of vegetation leachates: consequences for dissolved organic matter dynamics in Arctic environments. Biogeochemistry 164, 73–98. https://doi.org/10.1007/s10533-022-00925-9.

AMAP, 2017. Snow, Water, Ice and Permafrost in the Arctic (SWIPA) 2017.

Amon, R.M.W., Rinehart, A.J., Duan, S., et al., 2012. Dissolved organic matter sources in large Arctic rivers. Geochimica et Cosmochimica Acta 94, 217–237. https://doi.org/10.1016/j.gca.2012.07.015.

Berner, L.T., Massey, R., Jantz, P., et al., 2020. Summer warming explains widespread but not uniform greening in the Arctic tundra biome. Nature Communications 11, 1–12. https://doi.org/10.1038/s41467-020-18479-5.

Bowen, S.R., Gregorich, E.G., Hopkins, D.W., 2009. Biochemical properties and biodegradation of dissolved organic matter from soils. Biology and Fertility of Soils 45, 733–742. https://doi.org/10.1007/s00374-009-0387-6.

Brock, O., Helmus, R., Kalbitz, K., Jansen, B., 2020. Non-target screening of leaf litter-derived dissolved organic matter using liquid chromatography coupled to high-resolution mass spectrometry (LC-QTOF-MS). European Journal of Soil Science 71, 420–432. https://doi.org/10.1111/ejss.12894.

Catalán, N., Pastor, A., Borrego, C.M., et al., 2021. The relevance of environment vs. composition on dissolved organic matter degradation in freshwaters. Limnology & Oceanography 66, 306–320. https://doi.org/10.1002/lno.11606.

Cleveland, C.C., Nemergut, D.R., Schmidt, S.K., Townsend, A.R., 2007. Increases in soil respiration following labile carbon additions linked to rapid shifts in soil microbial community composition. Biogeochemistry 82, 229–240. https://doi.org/10.1007/s10533-006-9065-z.

Costa, O.Y.A., Raaijmakers, J.M., Kuramae, E.E., 2018. Microbial extracellular polymeric substances: ecological function and impact on soil aggregation. Frontiers in Microbiology 9, 1–14. https://doi.org/10.3389/fmicb.2018.01636.

Crow, S.E., Lajtha, K., Bowden, R.D., et al., 2009. Increased coniferous needle inputs accelerate decomposition of soil carbon in an old-growth forest. Ecological Management 258, 2224–2232. https://doi.org/10.1016/j.foreco.2009.01.014.

Crump, B.C., Kling, G.W., Bahr, M., Hobbie, J.E., 2003. Bacterioplankton community shifts in an Arctic lake correlate with seasonal changes in organic matter source. Applied and Environmental Microbiology 69, 2253–2268. https://doi.org/10.1128/AEM.69.4.2253-2268.2003.

Cuss, C.W., Guéguen, C., 2013. Distinguishing dissolved organic matter at its origin: size and optical properties of leaf-litter leachates. Chemosphere 92, 1483–1489. https://doi.org/10.1016/j.chemosphere.2013.03.062.

Cuss, C.W., Guéguen, C., 2012. Impacts of microbial activity on the optical and copper-binding properties of leaf-litter leachate. Frontiers in Microbiology 3, 1–10. https://doi.org/10.3389/fmicb.2012.00166.

Dinno, A., 2017. Package 'dunn.test.'. CRAN Repos 1–7.

Docherty, K.M., Young, K.C., Maurice, P.A., Bridgham, S.D., 2006. Dissolved organic matter concentration and quality influences upon structure and function of freshwater microbial communities. Microbial Ecology 52, 378–388. https://doi.org/10.1007/s00248-006-9089-x.

Drozdova, O.Y., Pokrovsky, O.S., Lapitskiy, S.A., et al., 2014. Decrease in zinc adsorption onto soil in the presence of EPS-rich and EPS-poor Pseudomonas aureofaciens. Journal of Colloid and Interface Science 435, 59–66. https://doi.org/10.1016/j.jcis.2014.08.025.

Elmendorf, S.C., Henry, G.H.R., Hollister, R.D., et al., 2012. Plot-scale evidence of tundra vegetation change and links to recent summer warming. Nature Climate Change 2, 453–457. https://doi.org/10.1038/nclimate1465.

Epstein, H.E., Myers-Smith, I., Walker, D.A., 2013. Recent dynamics of arctic and sub-arctic vegetation. Environmental Research Letters 8, 015040. https://doi.org/10.1088/1748-9326/8/1/015040.

Flemming, H.C., Wingender, J., 2010. The biofilm matrix. Nature Reviews Microbiology 8, 623–633. https://doi.org/10.1038/nrmicro2415.

Fouché, J., Christiansen, C.T., Lafrenière, M.J., et al., 2020. Canadian permafrost stores large pools of ammonium and optically distinct dissolved organic matter. Nature Communications 11. https://doi.org/10.1038/s41467-020-18331-w.

Fouché, J., Lafrenière, M.J., Rutherford, K., Lamoureux, S., 2017. Seasonal hydrology and permafrost disturbance impacts on dissolved organic matter composition in High Arctic headwater catchments. Arct Sci 3, 378–405. https://doi.org/10.1139/as-2016-0031.

Frey, K.E., Smith, L.C., 2005. Amplified carbon release from vast West Siberian peatlands by 2100. Geophysical Research Letters 32, 1–4. https://doi.org/10.1029/2004GL022025.

Gonsior, M., Schmitt-Kopplin, P., Bastviken, D., 2013. Depth-dependent molecular composition and photo-reactivity of dissolved organic matter in a boreal lake under winter and summer conditions. Biogeosciences 10, 6945–6956. https://doi.org/10.5194/bg-10-6945-2013.

González, A.G., Pokrovsky, O.S., Jiménez-Villacorta, F., et al., 2014. Iron adsorption onto soil and aquatic bacteria: XAS structural study. Chemical Geology 372, 32–45. https://doi.org/10.1016/j.chemgeo.2014.02.013.

González, A.G., Shirokova, L.S., Pokrovsky, O.S., et al., 2010. Adsorption of copper on Pseudomonas aureofaciens: protective role of surface exopolysaccharides. Journal of Colloid and Interface Science 350, 305–314. https://doi.org/10.1016/j.jcis.2010.06.020.

Heijmans, M.M.P.D., Magnússon, R., Lara, M.J., et al., 2022. Tundra vegetation change and impacts on permafrost. Nature Reviews Earth & Environment 3, 68–84. https://doi.org/10.1038/s43017-021-00233-0.

Hensgens, G., Lechtenfeld, O.J., Guillemette, F., et al., 2021. Impacts of litter decay on organic leachate composition and reactivity. Biogeochemistry 154, 99–117. https://doi.org/10.1007/s10533-021-00799-3.

Hunt, J.F., Ohno, T., 2007. Characterization of fresh and decomposed dissolved organic matter using excitation-emission matrix fluorescence spectroscopy and multiway analysis. Journal of Agricultural and Food Chemistry 55, 2121–2128. https://doi.org/10.1021/jf063336m.

Johansson, M., Åkerman, J., Keuper, F., et al., 2011. Past and present permafrost temperatures in the Abisko area: redrilling of boreholes. Ambio 40, 558–565. https://doi.org/10.1007/s13280-011-0163-3.

Jones, D.L., Eldhuset, T., De Wit, H.A., Swensen, B., 2001. Aluminium effects on organic acid mineralization in a Norway spruce forest soil. Soil Biol Biochem 33, 1259–1267. https://doi.org/10.1016/S0038-0717(01)00032-3.

Kaiser, K., Kalbitz, K., 2012. Cycling downwards - dissolved organic matter in soils. Soil Biol Biochem 52, 29–32. https://doi.org/10.1016/j.soilbio.2012.04.002.

Kalbitz, K., Meyer, A., Yang, R., Gerstberger, P., 2007. Response of dissolved organic matter in the forest floor to long-term manipulation of litter and throughfall inputs. Biogeochemistry 86, 301–318. https://doi.org/10.1007/s10533-007-9161-8.

Kalbitz, K., Schmerwitz, J., Schwesig, D., Matzner, E., 2003. Biodegradation of soil-derived dissolved organic matter as related to its properties. Geoderma 113, 273–291. https://doi.org/10.1016/S0016-7061(02)00365-8.

Kalbitz, K., Solinger, S., Park, J.-H., et al., 2000. Controls on the dynamics of dissolved organic matter in soil: a review. Soil Science 165, 277–304.

Kiikkilä, O., Kitunen, V., Smolander, A., 2005. Degradability of dissolved soil organic carbon and nitrogen in relation to tree species. FEMS Microbiology Ecology 53, 33–40. https://doi.org/10.1016/j.femsec.2004.08.011.

Koch, B.P., Dittmar, T., 2006. From mass to structure : an aromaticity index for high-resolution mass data of natural organic matter. Rapid Communications in Mass Spectrometry 20, 926–932. https://doi.org/10.1002/rcm.7433.

Kögel-Knabner, I, 2002. The macromolecular organic composition of plant and microbial residues as inputs to soil organic matter. Soil Biol Biochem 34, 139–162. https://doi.org/10.1016/S0038-0717(01)00158-4.

Lang, S.I., Cornelissen, J.H.C., Klahn, T., et al., 2009. An experimental comparison of chemical traits and litter decomposition rates in a diverse range of subarctic bryophyte, lichen and vascular plant species. Journal of Ecology 97, 886–900. https://doi.org/10.1111/j.1365-2745.2009.01538.x.

Manasypov, R.M., Vorobyev, S.N., Loiko, S.V., et al., 2015. Seasonal dynamics of organic carbon and metals in thermokarst lakes from the discontinuous permafrost zone of western Siberia. Biogeosciences 12, 3009–3028. https://doi.org/10.5194/bg-12-3009-2015.

Mann, P.J., Davydova, A., Zimov, N., et al., 2012. Controls on the composition and lability of dissolved organic matter in Siberia's Kolyma River basin. J Geophys Res Biogeosciences 117, 1–15. https://doi.org/10.1029/2011JG001798.

Mann, P.J., Eglinton, T.I., McIntyre, C.P., et al., 2015. Utilization of ancient permafrost carbon in headwaters of Arctic fluvial networks. Nature Communications 6, 1–7. https://doi.org/10.1038/ncomms8856.

Maria, E., Crançon, P., Lespes, G., Bridoux, M.C., 2019. Spatial variation in the molecular composition of dissolved organic matter from the podzol soils of a temperate pine forest. ACS Earth and Space Chemistry 3, 1685–1696. https://doi.org/10.1021/acsearthspacechem.9b00164.

Marschner, B., Kalbitz, K., 2003. Controls of bioavailability and biodegradability of dissolved organic matter in soils. Geoderma 113, 211–235. https://doi.org/10.1016/S0016-7061(02)00362-2.

Minor, E.C., Swenson, M.M., Mattson, B.M., Oyler, A.R., 2014. Structural characterization of dissolved organic matter: a review of current techniques for isolation and analysis. Environ Sci Process Impacts 16, 2064–2079. https://doi.org/10.1039/c4em00062e.

Morgalev, Y.N., Lushchaeva, I.V., Morgaleva, T.G., et al., 2017. Bacteria primarily metabolize at the active layer/permafrost border in the peat core from a permafrost region in western Siberia. Polar Biology 40, 1645–1659. https://doi.org/10.1007/s00300-017-2088-1.

Myers-Smith, I.H., Forbes, B.C., Wilmking, M., et al., 2011. Shrub expansion in tundra ecosystems: dynamics, impacts and research priorities. Environmental Research Letters 6, 045509. https://doi.org/10.1088/1748-9326/6/4/045509.

Nebbioso, A., Piccolo, A., 2013. Molecular characterization of dissolved organic matter (DOM): a critical review. Analytical and Bioanalytical Chemistry 405, 109–124. https://doi.org/10.1007/s00216-012-6363-2.

O'Donnell, J., Douglas, T., Barker, A., 2021. Changing biogeochemical cycles of organic carbon, nitrogen, phosphorus, and trace elements in arctic rivers. In: Arctic Hydrology, Permafrost and Ecosystems. Springer, pp. 315–348.

Olefeldt, D., Roulet, N.T., 2012. Effects of permafrost and hydrology on the composition and transport of dissolved organic carbon in a subarctic peatland complex. Journal of Geophysical Research: Biogeosciences 117, 1–15. https://doi.org/10.1029/2011JG001819.

Oleinikova, O.V., Shirokova, L.S., Drozdova, O.Y., et al., 2018. Low biodegradability of dissolved organic matter and trace metals from subarctic waters. Sci Total Environ 618, 174–187. https://doi.org/10.1016/j.scitotenv.2017.10.340.

Overland, J.E., Wang, M., 2013. When will the summer Arctic be nearly sea ice free? Geophysical Research Letters 40, 2097–2101. https://doi.org/10.1002/grl.50316.

Payandi-Rolland, D., Shirokova, L.S., Tesfa, M., et al., 2020. Dissolved organic matter biodegradation along a hydrological continuum in permafrost peatlands. Sci Total Environ 749, 141463. https://doi.org/10.1016/j.scitotenv.2020.141463.

Peacock, M., Evans, C.D., Fenner, N., et al., 2014. UV-visible absorbance spectroscopy as a proxy for peatland dissolved organic carbon (DOC) quantity and quality: considerations on wavelength and absorbance degradation. Environ Sci Process Impacts 16, 1445–1461. https://doi.org/10.1039/c4em00108g.

Pinsonneault, A.J., Moore, T.R., Roulet, N.T., 2016. Biodegradability of vegetation-derived dissolved organic carbon in a cool temperate ombrotrophic bog. Ecosystems 19, 1023–1036. https://doi.org/10.1007/s10021-016-9984-z.

Qualls, R.G., Haines, B.L., 1992. Biodegradability of dissolved organic matter in forest throughfall, soil solution, and stream water. Soil Science Society of America Journal 56, 578–586.

Rivas-Ubach, A., Liu, Y., Bianchi, T.S., et al., 2018. Moving beyond the van Krevelen diagram: a new stoichiometric approach for compound classification in organisms. Analytical Chemistry 90, 6152–6160. https://doi.org/10.1021/acs.analchem.8b00529.

Rosario-Ortiz, F.L., Korak, J.A., 2017. Oversimplification of dissolved organic matter fluorescence analysis: potential pitfalls of current methods. Environ Sci Technol 51, 759–761. https://doi.org/10.1021/acs.est.6b06133.

Serreze, M.C., Barrett, A.P., Stroeve, J.C., et al., 2009. The emergence of surface-based Arctic amplification. The Cryosphere 3, 11–19. https://doi.org/10.5194/tc-3-11-2009.

Shirokova, L.S., Bredoire, R., Rols, J.L., Pokrovsky, O.S., 2017. Moss and peat leachate degradability by heterotrophic bacteria: the fate of organic carbon and trace metals. Geomicrobiology Journal 34, 641–655. https://doi.org/10.1080/01490451.2015.1111470.

Shirokova, L.S., Pokrovsky, O.S., Kirpotin, S.N., et al., 2013. Biogeochemistry of organic carbon, CO2, CH4, and trace elements in thermokarst water bodies in discontinuous permafrost zones of Western Siberia. Biogeochemistry 113, 573–593. https://doi.org/10.1007/s10533-012-9790-4.

Speetjens, N.J., Tanski, G., Martin, V., et al., 2022. Dissolved organic matter characterization in soils and streams in a small coastal low-arctic catchment. Biogeosciences 19, 1–49.

Sturm, M., Racine, C., Tape, K., 2001. Increasing shrub abundance in the Arctic. Nature 411, 546–547. https://doi.org/10.1038/35079180.

Tape, K., Sturm, M., Racine, C., 2006. The evidence for shrub expansion in Northern Alaska and the Pan-Arctic. Global Change Biology 12, 686–702. https://doi.org/10.1111/j.1365-2486.2006.01128.x.

Van Der Kolk, H.J., Heijmans, M.M.P.D., Van Huissteden, J., et al., 2016. Potential Arctic tundra vegetation shifts in response to changing temperature, precipitation and permafrost thaw. Biogeosciences 13, 6229–6245. https://doi.org/10.5194/bg-13-6229-2016.

Van Hees, P.A.W., Jones, D.L., Finlay, R., et al., 2005. The carbon we do not see - the impact of low molecular weight compounds on carbon dynamics and respiration in forest soils: a review. Soil Biol Biochem 37, 1–13. https://doi.org/10.1016/j.soilbio.2004.06.010.

Van Hees, P.A.W., Jones, D.L., Godbold, D.L., 2002. Biodegradation of low molecular weight organic acids in coniferous forest podzolic soils, 34, 1261–1272.

Walker, M.D., Wahren, C.H., Hollister, R.D., et al., 2006. Plant community responses to experimental warming across the tundra biome. Proc Natl Acad Sci U S A 103, 1342–1346. https://doi.org/10.1073/pnas.0503198103.

Walvoord, M.A., Voss, C.I., Wellman, T.P., 2012. Influence of permafrost distribution on groundwater flow in the context of climate-driven permafrost thaw : example from Yukon Flats Basin. Alaska , United States 48, 1–17. https://doi.org/10.1029/2011WR011595.

Ward, CP, Cory, RM, 2015. Chemical composition of dissolved organic matter draining permafrost soils. Geochim Cosmochim Acta 167, 63–79.

Ward, C.P., Cory, R.M., 2016. Complete and partial photo-oxidation of dissolved organic matter draining permafrost soils. Environ Sci Technol 50, 3545–3553. https://doi.org/10.1021/acs.est.5b05354.

Weishaar, J.L., Aiken, G.R., Bergamaschi, B.A., et al., 2003. Evaluation of specific ultraviolet absorbance as an indicator of the chemical composition and reactivity of dissolved organic carbon. Environ Sci Technol 37, 4702–4708. https://doi.org/10.1021/es030360x.

Wickland, K.P., Neff, J.C., Aiken, G.R., 2007. Dissolved organic carbon in Alaskan boreal forest: sources, chemical characteristics, and biodegradability. Ecosystems 10, 1323–1340. https://doi.org/10.1007/s10021-007-9101-4.

Wingender, J., Neu, T., Flemming, H.C., 1999. What are bacterial extracellular polymeric substances?. In: Microbial Extracellular Polymeric Substances, pp. 1–19.

Wologo, E., Shakil, S., Zolkos, S., et al., 2021. Stream dissolved organic matter in permafrost regions shows surprising compositional similarities but negative priming and nutrient effects. Global Biogeochemical Cycles 35, 1–25. https://doi.org/10.1029/2020GB006719.

Zhao, Y.G., Cai, M.Q., Chen, X.H., et al., 2013. Analysis of nine food additives in wine by dispersive solid-phase extraction and reversed-phase high performance liquid chromatography. Food Research International 52, 350–358. https://doi.org/10.1016/j.foodres.2013.03.038.